Modeling photon propagation in biological tissues using a generalized Delta-Eddington phase function

W. Cong,[1] H. Shen,[1] A. Cong,[1] Y. Wang,[2] and G. Wang[1]
[1]*Biomedical Imaging Division, School of Biomedical Engineering and Sciences, Virginia Polytechnic Institute and State University, 1880 Pratt Drive, Suite 2000, Blacksburg, Virginia 24061, USA*
[2]*Computational Bioinformatics and Bio-imaging Laboratory, Department of Electrical and Computer Engineering, Virginia Polytechnic Institute and State University, 4300 Wilson Blvd., Suite 750, Arlington, Virginia 22203, USA*
(Received 5 June 2007; published 14 November 2007)

Photon propagation in biological tissue is commonly described by the radiative transfer equation, while the phase function in the equation represents the scattering characteristics of the medium and has significant influence on the precision of solution and the efficiency of computation. In this work, we present a generalized Delta-Eddington phase function to simplify the radiative transfer equation to an integral equation with respect to photon fluence rate. Comparing to the popular diffusion approximation model, the solution of the integral equation is highly accurate to model photon propagation in the biological tissue over a broad range of optical parameters. This methodology is validated by Monte Carlo simulation.

DOI: 10.1103/PhysRevE.76.051913 PACS number(s): 87.57.Gg, 42.62.Be, 42.68.Ay

I. INTRODUCTION

Photon propagation through scattering media has attracted a considerable interest for biomedical imaging applications. Optical molecular imaging techniques are applied to reveal molecular and cellular activities in vivo and study physiological and pathological processes in various small animal models [1]. Photon propagation in biological tissue is mainly affected by absorption and scattering. The light propagation model describes the interaction of photons with scattering and absorbing media, and is essential in biomedical optics for the development of imaging algorithms [2]. The radiative transfer equation (RTE) well describes the photon propagation in biological tissues [2,3]. A number of computational schemes were developed to solve RTE, including Monte Carlo (MC) simulation techniques [4], discrete ordinate methods [5,6], and so on [7]. Although MC simulation is a proven and popular stochastic method, which provides a highly accurate solution of the RTE, the high computational cost makes it an improper choice for dealing with typical inverse problems in the medical imaging field. The discrete ordinate method discretizes the RTE in different solid angle directions, and the resultant system of algebraic equations has to be solved iteratively, which is computationally inefficient and expensive in practice. The diffusion approximation (DA) is the most widely used as a photon propagation model because of its high computational efficiency, but it only works well in weakly absorbing and highly scattering media [8,9]. However, the bioluminescence and fluorescence proteins emit photons in the visible light spectrum, and the biological tissue presents significant photon absorption in this spectral region [10], resulting in a violation of the essential assumption of the DA. As a result, the DA model would generate a quite sizable discrepancy between the model prediction and real data. In this paper, we present a generalized Delta-Eddington phase function in RTE. Based on this new definition of the Delta-Eddington phase function, RTE can be significantly reduced to an integral equation for the photon fluence rate. The solution of the integral equation allows an accurate prediction to photon propagation in biological tissues over a broad range of optical parameters.

II. PHASE APPROXIMATION MODEL

RTE is an energy balance equation with respect to photon radiance and is expressed by [2,3]

$$\mathbf{v}\cdot\nabla L(\mathbf{r},\mathbf{v})+(\mu_a+\mu_s)L(\mathbf{r},\mathbf{v}) = \mu_s\oint_{S^2} L(\mathbf{r},\mathbf{v}')p(\mathbf{v}',\mathbf{v})d\mathbf{v}'+\frac{1}{4\pi}S(\mathbf{r}),\quad \mathbf{r}\in\Omega, \quad (1)$$

where Ω is the region of interest, $L(\mathbf{r},\mathbf{v})$ is the photon radiance at location $\mathbf{r}$ in the direction of unit vector $\mathbf{v}$ [W mm^{-2} sr^{-1}], $S(\mathbf{r})$ is the isotropic source [W mm^{-3}], μ_s is the scattering coefficient [mm^{-1}], and μ_a is the absorption coefficient [mm^{-1}]. The scattering phase function $p(\mathbf{v},\mathbf{v}')$ gives the probability of a photon coming in the direction $\mathbf{v}'$ being scattered into the direction $\mathbf{v}$. The exact phase function is generally unknown in practice. Several frequently used phase functions are only its approximations, such as the Delta-Eddington function and Henyey-Greenstein function. Biological tissue strongly scatters photon in the forward direction [11]. Hence, the phase function can be well modeled by a generalized Delta-Eddington function [12,13] as follows:

$$p(\mathbf{v}\cdot\mathbf{v}')=\frac{1}{4\pi}(1-f)+\frac{1}{2\pi}f\delta(1-\mathbf{v}\cdot\mathbf{v}'), \quad (2)$$

where $f\in[-1,+1]$ is the weight factor measuring the anisotropy of photon scattering, which is called the anisotropy weight. The phase function is a linear combination between the isotropic scattering and the strongly peaked forward scattering. The original Delta-Eddington phase function rigidly defines the parameter f as a fixed value g, where g is an anisotropic factor defined as the mean value of the cosine of the scattering angles. In contrast to the conventional interpretation, the generalized Delta-Eddington function requires that

the anisotropy weight be related to the photon absorbing and scattering in the medium, and the optical properties of medium are characterized by the anisotropy weight f along with the absorption and scattering coefficients.

Substitution of Eq. (2) into Eq. (1) yields

$$\mathbf{v}\cdot\nabla L(\mathbf{r},\mathbf{v})+\tilde{\mu}_t L(\mathbf{r},\mathbf{v})=\frac{1}{4\pi}[\tilde{\mu}_s\Phi(\mathbf{r})+S(\mathbf{r})],\quad \mathbf{r}\in\Omega, \tag{3}$$

where $\tilde{\mu}_s=(1-f)\mu_s$, $\tilde{\mu}_t=\tilde{\mu}_s+\mu_a$, and the photon fluence rate $\Phi(\mathbf{r})$ is defined by

$$\Phi(\mathbf{r})=\oint_{S^2} L(\mathbf{r},\mathbf{v})d\mathbf{v}. \tag{4}$$

Equation (3) is a linear, first-order differential equation describing the photon propagation through a heterogeneous medium, and the solution $L(\mathbf{r},\mathbf{v})$ can be formulated as [14]

$$\begin{aligned}L(\mathbf{r},\mathbf{v})=&\frac{1}{4\pi}\int_0^R[\tilde{\mu}_s(\mathbf{r}-\rho\mathbf{v})\Phi(\mathbf{r}-\rho\mathbf{v})+S(\mathbf{r}-\rho\mathbf{v})]\\&\times\exp\left(-\int_0^\rho\tilde{\mu}_t(\mathbf{r}-t\mathbf{v})dt\right)d\rho+L(\mathbf{r}-R\mathbf{v},\mathbf{v})\\&\times\exp\left(-\int_0^R\tilde{\mu}_t(\mathbf{r}-t\mathbf{v})dt\right),\end{aligned} \tag{5}$$

where R is a scalar so that $\mathbf{r}-R\mathbf{v}\in\partial\Omega$, representing the distance from point $\mathbf{r}$ to the boundary $\partial\Omega$ along the direction $\mathbf{v}$. Integration of Eq. (5) over all the solid angles results in the following integral formula:

$$\begin{aligned}\Phi(\mathbf{r})=&\frac{1}{4\pi}\oint_{S^2}\int_0^R[\tilde{\mu}_s(\mathbf{r}-\rho\mathbf{v})\Phi(\mathbf{r}-\rho\mathbf{v})+S(\mathbf{r}-\rho\mathbf{v})]\\&\times\exp\left(-\int_0^\rho\tilde{\mu}_t(\mathbf{r}-t\mathbf{v})dt\right)d\rho d\mathbf{v}+\oint_{S^2}L(\mathbf{r}-R\mathbf{v},\mathbf{v})\\&\times\exp\left(-\int_0^R\tilde{\mu}_t(\mathbf{r}-t\mathbf{v})dt\right)d\mathbf{v}.\end{aligned} \tag{6}$$

In the case of an optical experiment in a totally dark environment, which no external photon travels in an inward direction on the boundary $\partial\Omega$, $L(\mathbf{r}-R\mathbf{v},\mathbf{v})$ in Eq. (6) would vanish for matched refractive indices on the boundary. However, since the refractive index n_{tissue} in biological tissues is higher than the refractive index n_{air} of the surrounding air, a fraction of photons will be internally reflected at the boundary. In this case, $L(\mathbf{r}-R\mathbf{v},\mathbf{v})$ describes the contribution from the reflected photons on the boundary, and the reflected radiance $L(\mathbf{r}-R\mathbf{v},\mathbf{v})$ on the boundary can be approximated by $[r_d/4\pi(1+r_d)]\Phi(\mathbf{r})$ based on the relation between photon transmission and reflection on boundary, where the internal reflection coefficient r_d can be calculated from $r_d=-1.4399\eta^{-2}+0.7099\eta^{-1}+0.6681+0.0636\eta$ for relative refractive index $\eta=n_{tissue}/n_{air}$ [13]. Furthermore, with a variable transformation from the polar coordinates $\mathbf{r}-\rho\mathbf{v}$ to the Cartesian coordinates $\mathbf{r}'$, an integral equation with respect to photon fluence rate is obtained,

$$\begin{aligned}\Phi(\mathbf{r})=&\frac{1}{4\pi}\int_\Omega[\tilde{\mu}_s(\mathbf{r}')\Phi(\mathbf{r}')+S(\mathbf{r}')]G(\mathbf{r},\mathbf{r}')d\mathbf{r}'\\&-\frac{r_d}{4\pi(1+r_d)}\oint_{\partial\Omega}\Phi(\mathbf{r}')G(\mathbf{r},\mathbf{r}')\boldsymbol{\beta}\cdot\mathbf{n}d\mathbf{r}',\end{aligned} \tag{7}$$

where

$$G(\mathbf{r},\mathbf{r}')=\frac{1}{|\mathbf{r}-\mathbf{r}'|^2}\exp\left(-\int_0^{|\mathbf{r}-\mathbf{r}'|}\tilde{\mu}_t(\mathbf{r}-t\boldsymbol{\beta})dt\right),$$

unit vector $\boldsymbol{\beta}=(\mathbf{r}-\mathbf{r}')/|\mathbf{r}-\mathbf{r}'|$, and $\mathbf{n}$ is the outward unit normal at $\mathbf{r}-R\boldsymbol{\beta}$ on the boundary. Equation (7) is a well-posed integral equation of the second kind, and allows an accurate prediction to photon propagation in biological tissues. For simplicity, we call Eq. (7) the phase approximation (PA) equation because it is derived from an approximate phase function. $\tilde{\mu}_s$ and $\tilde{\mu}_t$ (or, equivalently, μ_a, μ_s, and f) in Eq. (7) represent the optical parameters. When the absorption coefficient μ_a and scattering coefficient μ_s in the tissue are unknown, we can directly determine the optical parameters $\tilde{\mu}_s$ and $\tilde{\mu}_t$ using optical tomography techniques based on Eq. (7) [15]. If the absorption coefficient μ_a, scattering coefficient μ_s, and conventional anisotropic factor g in the tissue are known, based on a simple homogenous numerical phantom, such as a spherical or cylindrical object, with a known light source setting, the photon fluence rate on the boundary of the phantom can be generated using Monte Carlo simulation with a appropriate phase function, e.g., the Henyey-Greenstein phase function [16]. Then, a single parameter optimization can be performed to determine the anisotropy weight f by matching the photon fluence rate on the phantom boundary obtained from the phase approximation model to the Monte Carlo simulation results.

III. NUMERICAL EXPERIMENTS

To compute the photon fluence rate from Eq. (7), the region of interest Ω is discretized into finite elements with N vertex nodes and the photon fluence rate $\Phi(\mathbf{r})$ is approximated in terms of nodal-based basis functions $\varphi_j(\mathbf{r})(j=1,2,\ldots,N)$ [17],

$$\Phi(\mathbf{r})=\sum_{j=1}^{N}\Phi(\mathbf{r}_j)\varphi_j(\mathbf{r}). \tag{8}$$

Substituting Eq. (8) into Eq. (7), we obtain the following matrix equation:

$$\{\boldsymbol{\Phi}\}=\mathbf{M}\{\boldsymbol{\Phi}\}+\mathbf{B}\{\boldsymbol{\Phi}\}+\{\mathbf{S}\}, \tag{9}$$

where $\{\boldsymbol{\Phi}\}$ consists of photon fluence rate values at the nodes in Ω; $\mathbf{M}$, $\mathbf{B}$, and $\{\mathbf{S}\}$ represent the corresponding discrete integral kernels in Eq. (7), with the components of the matrices defined by

$$m_{i,j}=\frac{1}{4\pi}\int_\Omega\tilde{\mu}_s(\mathbf{r}')\varphi_j(\mathbf{r}')G(\mathbf{r}_i,\mathbf{r}')d\mathbf{r}',$$

TABLE I. Optical parameters used in the numerical experiments.

μ_a (mm^{-1})	μ_s (mm^{-1})	$\mu_s(1-g)/\mu_a$	$g=0.9$	$\eta=1.37$	f
0.35	12.50	3.57	0.9	1.37	0.907
0.20	14.50	7.25	0.9	1.37	0.925
0.016	9.0	56.25	0.9	1.37	0.957
0.008	8.0	100.0	0.9	1.37	0.961

$$b_{i,j} = \frac{r_d}{4\pi(1+r_d)} \oint_{\partial\Omega} \varphi_j(\mathbf{r}')G(\mathbf{r}_i,\mathbf{r}')(\boldsymbol{\beta}\cdot\mathbf{n})d\mathbf{r}',$$

$$s_i = \frac{1}{4\pi}\int_{\Omega} S(\mathbf{r}')G(\mathbf{r}_i,\mathbf{r}')d\mathbf{r}'. \tag{10}$$

Solving the matrix equation (9), the photon fluence rate is given by

$$\{\mathbf{\Phi}\} = \mathbf{K}\{\mathbf{S}\}, \tag{11}$$

where $\mathbf{I}$ is a unit matrix and $\mathbf{K}=(\mathbf{I}-\mathbf{M}-\mathbf{B})^{-1}$. Equation (11) is ready to be numerically implemented to compute the photon fluence rate.

Extensive numerical experiments were conducted to verify the proposed method. In our experiments, a spherical phantom of radius 10 mm was used to determine the anisotropy weight f based on known optical parameter: absorption, scattering coefficients, and anisotropic factor g. A spherical source of radius 0.6 mm was embedded into the spherical phantom. The centers of the source located at (2.5, 2.5, 0.0), and the light source had the power of 10 nanowatts. The phantom was then discretized into 65 775 tetrahedral elements and 12 044 nodes. A total of 2108 virtual detectors were distributed over the phantom surface to record the photon fluence rate. MC simulation with a Henyey-Greenstein phase function was performed with known optical parameters (μ_a, μ_s, and g) to obtain the photon fluence rate on detectors. The anisotropy weight f is estimated by matching the solution of the PA equation (7) to the photon fluence rate obtained from the MC simulation. This procedure was performed for four sets of optical parameters with various reduced scattering albedos defined by $\mu_s(1-g)/\mu_a$ to obtain the anisotropy weights. The computed anisotropy weights f were shown in Table I.

We further performed the numerical experiments to compare the accuracy between the MC, PA, and DA models. A cylindrical phantom of diameter 20 mm and height 20 mm was used. A spherical source of radius 1.0 mm was placed at (−4.0, 0.0, 10.0) in the cylindrical phantom. The phantom was then discretized into 25 335 tetrahedral elements and 4833 nodes for the numerical computation of the PA and DA models. A total of 1226 virtual detectors were allocated over the surface of the phantom to record the photon fluence rate. The DA model coupled with the Robin boundary condition [9]. The MC simulation used the Henyey-Greenstein phase function. The PA, DA, and MC simulators were implemented to generate the photon fluence rates at detectors on the boundary of the phantom based on the four sets of optical parameters in Table I. Figures 1(a), 1(b), 2(a), 2(b), 3(a), 3(b), 4(a), and 4(b) presented the comparison between the solution of PA, DA, and the MC simulation for the reduced scattering albedos 3.57, 7.25, 56.25, and 100, respectively. These results show that the solutions obtained via the PA equation (7) are in excellent agreement with the results from the MC simulation with a relative error below 3.7%, herein the relative error is defined as $\Sigma_{detectors}|\Phi_{MC}-\Phi_{PA}|/\Sigma_{detectors}\Phi_{MC}$. In contrast, we found that the solution of the DA model was less accurate for relatively small reduced scattering albedo. For example, there are major discrepancies between DA prediction and MC simulation for the reduced scattering albedos 3.57 and 7.25, where the relative errors were as high as 31.2% and 14.6%, respectively, as shown in Figs. 1(b) and 2(b). As expected, for higher reduced scattering albedos 56.25 and 100 the DA model gave good performance with relative errors 4.1% and 3.8%, re-

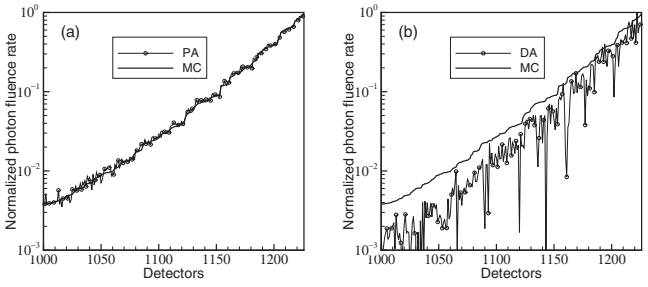

FIG. 1. Comparison of the detected photon fluence rates obtained from the MC simulation, PA, and DA models. (a) PA vs MC. (b) DA vs MC with optical parameters $\mu_a=0.35$ mm^{-1}, $\mu_s=12.5$ mm^{-1}, $g=0.9$, $f=0.907$, and $\eta=1.37$. Detectors are sorted by the increasing order of photon fluence rates of MC simulation.

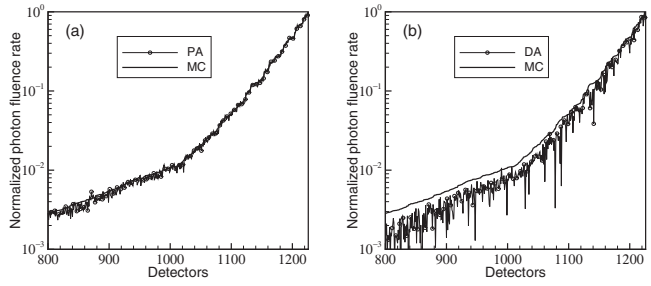

FIG. 2. Comparison of the detected photon fluence rates obtained from the MC simulation, PA, and DA models. (a) PA vs MC. (b) DA vs MC with optical parameters $\mu_a=0.20$ mm^{-1}, $\mu_s=14.5$ mm^{-1}, $g=0.9$, $f=0.925$, and $\eta=1.37$. Detectors are sorted by the increasing order of photon fluence rates of MC simulation.

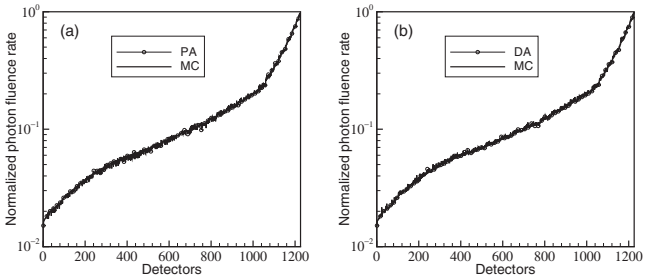

FIG. 3. Comparison of the detected photon fluence rates obtained from the MC simulation, PA, and DA models. (a) PA vs MC. (b) DA vs MC with optical parameters $\mu_a=0.016\ \mathrm{mm}^{-1}$, $\mu_s=9.0\ \mathrm{mm}^{-1}$, $g=0.9$, $f=0.957$, and $\eta=1.37$. Detectors are sorted by the increasing order of photon fluence rates of MC simulation.

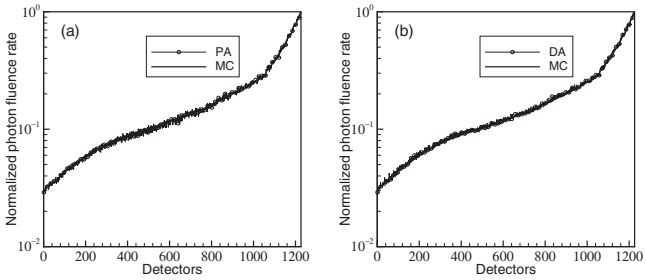

FIG. 4. Comparison of the detected photon fluence rates obtained from the MC simulation, PA, and DA models. (a) PA vs MC. (b) DA vs MC with optical parameters $\mu_a=0.008\ \mathrm{mm}^{-1}$, $\mu_s=8.0\ \mathrm{mm}^{-1}$, $g=0.9$, $f=0.961$, and $\eta=1.37$. Detectors are sorted by the increasing order of photon fluence rates of MC simulation.

spectively, as shown in Figs. 3(b) and 4(b). The numerical experiments show that the photon fluence rate obtained from the PA equation is more accurate than the results from the DA model over a broad range of optical parameters. The computational cost of the PA equation is much lower than the cost of the direct computational method of RTE. The computational time of the PA equation was about eight minutes, while the DA model cost about three minutes in our numerical experiments. In addition, it is clear that the reconstructed anisotropy weight f from known absorption, scattering coefficients, and anisotropic factor g is independent of the geometrical shape of media.

IV. DISCUSSION AND CONCLUSIONS

We have presented a generalized Delta-Eddington phase function, which is a linear combination between the isotropic scattering and the strongly peaked forward scattering with the anisotropy weight f as a coefficient. The function allows an accurate description for the anisotropic scattering characteristic of medium with an optimal anisotropy weight. Different from the original Delta-Eddington phase function that the anisotropy weight is independent of the absorbing and scattering coefficients and is rigidly fixed to the anisotropic factor g, our proposed generalized Delta-Eddington phase function requires that the anisotropy weight be related to the photon absorbing and scattering coefficients in the medium. The anisotropy weight can be determined by optical tomography techniques for unknown optical parameters or MC simulation from known absorption, scattering coefficients, and conventional anisotropic factor g. In the phase approximation model, the optical properties of medium are described by the anisotropy weight f along with the absorption and scattering coefficients instead of conventionally anisotropic factor g. Using the generalized Delta-Eddington phase function, the five-dimensional RTE was significantly simplified to a three-dimensional integral equation with respect to the photon fluence rate. The computational complexity of the PA equation is comparable to that of the DA model. Compared to the diffusion approximation model derived from the first-order approximation of the photon radiance, the phase approximation model is based on the exact computation of the photon radiance. The numerical experiments have demonstrated that the solution of the PA equation is highly accurate over a broad range of optical parameters by comparing to the results of MC simulation in numerical phantom experiments, while the DA model only works well in a highly scattering and weakly absorbing medium. Based on our promising numerical data, the proposed method has a great potential for optical tomography, bioluminescence tomography, fluorescence tomography, and other optical imaging applications.

ACKNOWLEDGMENTS

This work was partially supported by the National Institutes of Health under Grants No. EB001685, No. EB006036, No. CA127189, No. EB000830, and No. NS29525.

[1] V. Ntziachristos, J. Ripoll, L. H. Wang, and R. Weissleder, Nat. Biotechnol. **23**, 313 (2005).
[2] A. J. Welch and M. J. C. van Gemert, *Optical and Thermal Response of Laser-Irradiated Tissue* (Plenum Press, New York, 1995).
[3] A. Ishimaru, *Wave Propagation and Scattering in Random Media* (Academic, New York, 1978), Vol. 1.
[4] L. H. Wang, S. L. Jacques, and L. Q. Zheng, Comput. Methods Programs Biomed. **47**, 131 (1995).
[5] S. Chandrasekhar, *Radiative Transfer* (Dover Publications, New York, 1960).
[6] G. S. Abdoulaev and A. H. Hielscher, J. Electron. Imaging **12**, 594 (2003).
[7] D. Klose and E. W. Larsen, J. Comput. Phys. **220**, 441 (2006).
[8] S. T. Flock, M. S. Patterson, B. C. Wilson, and D. R. Wyman, IEEE Trans. Biomed. Eng. **36**, 1162 (1989).
[9] M. Schweiger, S. R. Arridge, M. Hiraoka, and D. T. Delpy, Med. Phys. **22**, 1779 (1995).

[10] R. Weissleder and V. Ntziachristos, Nat. Med. **9**, 123 (2003).
[11] W. F. Cheong, S. A. Prahl, and A. J. Welch, IEEE J. Quantum Electron. **26**, 2166 (1990).
[12] J. H. Joseph, W. J. Wiscombe, and J. A. Weinman, J. Atmos. Sci. **33**, 2452 (1976).
[13] R. A. J. Groenhuis, H. A. Ferwerda, and J. J. Ten Bosch, Appl. Opt. **22**, 2456 (1983).
[14] F. Natterer and F. Wübbeling, *Mathematical Methods in Image Reconstruction* (SIAM, Philadelphia, 2001).
[15] S. R. Arridge, Inverse Probl. **15**, R41 (1999).
[16] L. C. Henyey and J. L. Greenstein, Astrophys. J. **93**, 70 (1941).
[17] S. S. Rao, *The Finite Element Method in Engineering* (Butterworth-Heinemann, Boston, 1999).